



RESEARCH ARTICLE

*Liver and Biliary Tract Physiology/Pathophysiology*

## Matrix stiffness and shear stresses modulate hepatocyte functions in a fibrotic liver sinusoidal model

Wang Li,<sup>1,2,3,4</sup> Peiwen Li,<sup>1,2,3,4</sup> Ning Li,<sup>1,2,3,4</sup> Yu Du,<sup>1,2,3,4</sup> Shouqin Lü,<sup>1,2,3,4</sup>  David Elad,<sup>5</sup> and  Mian Long<sup>1,2,3,4</sup>

<sup>1</sup>Center for Biomechanics and Bioengineering, Institute of Mechanics, Chinese Academy of Sciences, Beijing, People's Republic of China; <sup>2</sup>Key Laboratory of Microgravity (National Microgravity Laboratory), Institute of Mechanics, Chinese Academy of Sciences, Beijing, People's Republic of China; <sup>3</sup>Beijing Key Laboratory of Engineered Construction and Mechanobiology, Institute of Mechanics, Chinese Academy of Sciences, Beijing, People's Republic of China; <sup>4</sup>School of Engineering Sciences, University of Chinese Academy of Sciences, Beijing, People's Republic of China; and <sup>5</sup>Department of Biomedical Engineering, Faculty of Engineering, Tel Aviv University, Tel Aviv, Israel

### Abstract

Extracellular matrix (ECM) rigidity has important effects on cell behaviors and increases sharply in liver fibrosis and cirrhosis. Hepatic blood flow is essential in maintaining hepatocytes' (HCs) functions. However, it is still unclear how matrix stiffness and shear stresses orchestrate HC phenotype in concert. A fibrotic three-dimensional (3-D) liver sinusoidal model is constructed using a porous membrane sandwiched between two polydimethylsiloxane (PDMS) layers with respective flow channels. The HCs are cultured in collagen gels of various stiffnesses in the lower channel, whereas the upper channel is pre-seeded with liver sinusoidal endothelial cells (LSECs) and accessible to shear flow. The results reveal that HCs cultured within stiffer matrices exhibit reduced albumin production and cytochrome *P450* (CYP450) reductase expression. Low shear stresses enhance synthetic and metabolic functions of HC, whereas high shear stresses lead to the loss of HC phenotype. Furthermore, both mechanical factors regulate HC functions by complementing each other. These observations are likely attributed to mechanically induced mass transport or key signaling molecule of hepatocyte nuclear factor 4 $\alpha$  (HNF4 $\alpha$ ). The present study results provide an insight into understanding the mechanisms of HC dysfunction in liver fibrosis and cirrhosis, especially from the viewpoint of matrix stiffness and blood flow.

**NEW & NOTEWORTHY** A fibrotic three-dimensional (3-D) liver sinusoidal model was constructed to mimic different stages of liver fibrosis in vivo and to explore the cooperative effects of matrix stiffness and shear stresses on hepatocyte (HC) functions. Mechanically induced alterations of mass transport mainly contributed to HC functions via typical mechanosensitive signaling.

*hepatocytes; liver fibrosis; matrix stiffness; shear flow; three-dimensional liver sinusoidal model*

### INTRODUCTION

The liver serves as one of the most critical organs in many processes of drug metabolism and detoxification (1, 2). As the largest visceral organ, the liver receives dual blood supply from portal vein and hepatic artery (3). A liver sinusoid, the elementary building block, is composed of parenchymal hepatocytes (HCs) and nonparenchymal cells (NPCs) that form two flow channels (sinusoidal microvasculature and space of Disse) within a three-dimensional (3-D) extracellular matrix (ECM) microenvironment. Thus, the HCs interact with liver sinusoidal endothelial cells (LSECs), hepatic stellate cells (HSCs), Kupffer cells (KCs), and leukocytes (4). Liver diseases, initiated by alcohol abuse, obesity, diabetes,

or chronic infection of hepatitis B virus (HBV) or hepatitis C virus (HCV), promote proinflammatory cytokine secretion by KCs and trigger the transition of HSCs from a quiescent to an activated state (5, 6). Activated HSCs proliferate, migrate, and produce a large quantity of ECM, including collagen types I and III, laminin, and hyaluronic acid (HA) (7–9). Overexpression of ECM induces dedifferentiation of hepatic cells and further activates the HSCs and followed by the positive feedback to propagate fibrotic response (7, 10, 11).

In a fibrotic liver, the ECM content is considerably increased up to 10-fold and leads to an altered microenvironment (12, 13). The extracellular microenvironment is essential in hepatic functions and provides not only biochemical but also mechanical cues to influence cellular phenotype



and behavior (14–16). Among the various mechanical cues, there is increased evidence that the ECM rigidity has a profound effect on HC spreading, proliferation, and dedifferentiation (17, 18). Different approaches have been developed to determine the stiffness. The rigidity of normal or pathological liver tissue was estimated via elastography (19, 20), rheometry (21, 22), and atomic force microscopy (AFM) (23), but the range of the measured data is wide, from 0.15 to 20 kPa. Nevertheless, all laboratory studies revealed that the stiffness for liver cirrhosis was at least twofold larger than that of a normal liver. To mimic this fibrotic or even cirrhotic process in vitro, HCs are usually seeded on polyacrylamide gels of tunable rigidity or on substrates utilizing decellularized liver scaffold for keeping those native growth factors in position (23, 24). Although these models or modules are simple to construct and operate, conventional monocultures of HC cannot adequately replicate the in vivo 3-D cellular microenvironments in liver. Even with a newly developed coculture system by integrating HCs with LSECs, HSCs and KCs on elasticity-tunable polyelectrolyte multilayers (PEMs) (12), the hemodynamic flow is absent, and it is hard to mimic in vivo blood flow.

Sinusoidal or interstitial blood flow in liver sinusoids is essential for oxygen and nutrient transport to HCs. Defenestration and capillarization of LSECs occur early in liver fibrosis development, limiting macromolecular or solute exchange across the endothelium and causing relative hypoxia (25, 26). Several liver diseases before cirrhosis are often accompanied by portal hypertension owing to increased intrahepatic vascular resistance (27), leading to significant reduction in blood velocity compared with healthy controls and disruption of the sinusoidal microcirculation (28). Meanwhile, cell survival, retention of metabolic activities, and functional polarization of HC are improved at physiological oxygen concentration when cultured on gas-permeable membrane (29). In the reported static in vitro cultures, the drug concentration used to demonstrate metabolic responses was usually higher than in in vivo plasma concentration to achieve similar effects (30–32). Therefore, the cellular effects in the in vitro culture may not reflect what happens in vivo. To mimic physiological blood flow and avoid excessive accumulation of metabolites, fluid flow, or perfusion is incorporated into HC culture in vitro (33–36).

Shear flow enhances albumin and urea syntheses significantly and maintains high expressions of nuclear factors and P450 enzymes required for drug metabolism (37). Interestingly, high shear stresses are detrimental to HC, as albumin production in the bioreactor declines considerably at high flow rates (38). The impact of fluid flow on HC functions was estimated using a rocking platform (39), a cone and plate rheometer (37, 40), and a flow chamber (41). The in vivo HCs are shielded from the direct stresses of sinusoidal blood flow but are exposed to the interstitial flow in the space of Disse that is filtered through the leaky fenestrae of LSECs. Accordingly, it is necessary to separate the HCs from direct exposure to flow, as seen in those mimicking in vivo hepatic flow, by using porous membranes (42), PEMs (43), and collagen gels (44).

Matrix stiffness and shear stresses are crucial in regulating HC dedifferentiation with a loss of liver-specific functions and metabolic enzyme activity in vitro. However, few studies

have examined how these two mechanical factors orchestrate HC phenotype in concert. In our previous study (45), we have developed an in vitro 3-D microfluidic sinusoidal coculture model by integrating NPCs and shear flow to recapitulate the complicated structure and the microenvironment of liver sinusoid. Here, we further improved this model by varying matrix stiffness with collagen I to mimic ECM deposition during the progress of liver fibrosis to explore the superimposed effects of matrix stiffness and shear stresses on synthetic and metabolic functions of HCs.

## MATERIALS AND METHODS

### Microfluidic Device Fabrication

A microfluidic device was fabricated using soft lithography as described previously (45). Briefly, a silicon-wafer SU-8 template (Capital Bio Corporation, Beijing, China) served as negative molds to generate the top and bottom layers of the device using polydimethylsiloxane (PDMS; Sylgard 184, Dow Corning, MI). If not mentioned otherwise, the main flowing zones of both upper and lower channels were equally sized with  $H \times W \times L = 100 \mu\text{m} \times 1 \text{mm} \times 10 \text{mm}$ , in which two sets of inlet and outlet ports were punched into the top PDMS layer. A 0.4- $\mu\text{m}$ -pore-sized polyethylene terephthalate (PET) membrane ( $4 \times 10^6$  pores/ $\text{cm}^2$ ; 10- $\mu\text{m}$ -thick) obtained from a transwell membrane insert (BD Biosciences, NJ) was cut into the desired shape and used to cover the lower channel. After treating the top and bottom layers with a Plasma Sputtering Pump (Yilibotong, China) for 1 min, the two PDMS layers and PET membrane were aligned and brought in conformal contact. The integrated device was UV-sterilized for 30 min, and both channels were coated with 100  $\mu\text{g}/\text{mL}$  collagen I at 37°C overnight before use (Fig. 1A).

### Isolation of Primary Hepatocytes

Murine HCs were isolated from 6- to 8-wk-old C57BL/6 mouse (Vital River Laboratories, Beijing, China) using a two-step collagenase perfusion protocol previously described (45, 46). The experimental protocol was approved by the Institutional Animal and Medicine Ethical Committee at the Institute of Mechanics of the Chinese Academy of Sciences. Briefly, the liver was perfused with buffer of EGTA (Sigma-Aldrich, MO) and heparin sodium (Sigma-Aldrich) at 5 mL/min, 37°C for 5 min via the portal vein. Subsequently, the liver was further perfused with collagenase IV (Sigma-Aldrich) for 5 min. Then, the liver was dissociated in collagenase IV solution and filtered with a 70- $\mu\text{m}$  cell strainer. The collected HCs were centrifuged at 54  $g$  for 2 min. The isolated HCs were used for experiment, with a viability >90%, as screened by trypan blue (Solarbio, China) stain assay.

### Cell Seeding inside the Device

Human hepatocellular carcinoma cell lines, C3A and HepG2, were obtained from American Type Culture Collection (ATCC, VA). Human LSEC line, human hepatic sinusoidal endothelial cells (HSECs) from ScienCell Research Laboratories (CA), was a kind gift from Dr. Yanan Du (Tsinghua University, Beijing, China). These cell lines were maintained in Dulbecco's modified Eagle medium (DMEM; Hyclone, UT). The culture medium was

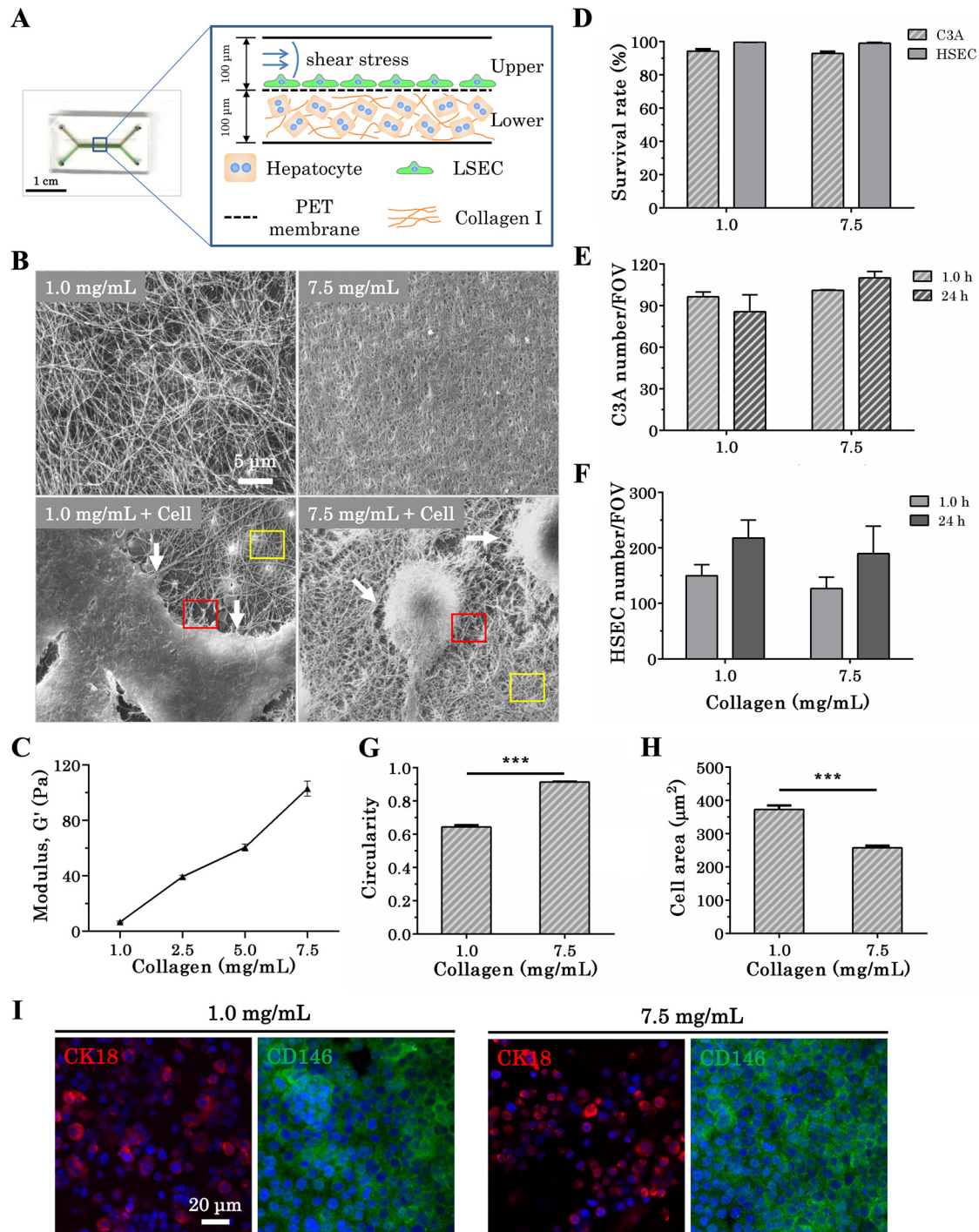


**Figure 1.** Establishment of a fibrotic three-dimensional (3-D) liver sinusoidal model. **A:** schematic of perfused co-culture of hepatocytes (HCs) and liver sinusoidal endothelial cells (LSECs) in a microfluidic sinusoidal model that was composed of two 100- $\mu\text{m}$ -high channels separated by a 10- $\mu\text{m}$ -thick porous polyethylene terephthalate (PET) membrane. Shear flow was infused into the upper channel lined with LSECs, whereas HCs premixed with collagen I solution were seeded in the lower channel. **B:** typical scanning electron microscopy (SEM) images of collagen gel network with/without HCs (C3A cells) at different collagen concentrations. White arrows indicated remodeled collagen networks, and red and yellow boxes denoted collagen fibers around cells and those far away from the cells, respectively. **C:** storage modulus of freshly polymerized samples at each collagen concentration. **D:** survival rate of C3A cells ( $n=15$ ) and hepatic sinusoidal endothelial cells (HSECs;  $n=15$ ) cultured in this sinusoidal model. Also denoted is the proliferation of C3A cells ( $n=3$ ) (**E**) and HSECs ( $n=3$ ) (**F**) after 24-h culture in various conditions. FOV, field of view. Cell area ( $n=9$ ) (**G**) and circularity ( $n=9$ ) (**H**) of C3A cells cultured in different collagen gels. **I:** immunofluorescence images stained for cytokeratin 18 (CK18) and cluster of differentiation 146 (CD146). Nuclei were shown by Hoechst staining. Data are presented as means  $\pm$  SE, and statistical analysis was conducted by Mann–Whitney test. \*\*\* $P < 0.001$ .  $n$ , number of samples.



supplemented with 10% fetal bovine serum (FBS; Gibco, CA) and 100 U/mL penicillin and 100 µg/mL streptomycin (Hyclone). Cells were passaged with 0.25% trypsin routinely once reaching 90% confluence. An HSEC suspension was prepared at a final concentration of  $1.0 \times 10^7$  cells/mL and then introduced into the upper channel using a pipette tip. Matrices with various stiffnesses were created from rat tail collagen type I (Corning, NY) at a concentration of 1.0, 2.5, 5.0, or 7.5 mg/mL. The resulted collagen solution was kept on ice before inducing polymerization with neutralizing NaOH (0.4M). Neutralized collagen was then gently mixed with primary HCs, C3A, or HepG2 suspension in a final concentration of  $1.0 \times 10^7$  cells/mL. The mixture was finally pipetted into the lower channel. The device was placed at 37°C for 30 min to implement collagen gel formation, resulting in embedding of HC into collagen gel in the lower channel. In the collagen I-free model, HCs were inoculated into the lower channel at the same cell density without being premixed with the collagen solution. After an additional 24 h, the upper channel was exposed to flow-induced shear stresses ( $\tau$ ),

$$\tau = (6\mu Q)/(WH^2) \quad (1)$$

where  $\mu$  is the fluid solution viscosity,  $Q$  is the flow rate, and  $W$  and  $H$  are the width and height of the microfluidic channel, respectively. Because LSECs were estimated to experience shear stresses of 0.1–0.5 dyn/cm<sup>2</sup> (45), we introduced a variety of flow rates (e.g., 0, 1.0, 5.0, and 10.0 µL/min) that resulted in shear stresses of 0, 0.1, 0.5, and 1.0 dyn/cm<sup>2</sup> within the upper channel, by using a PHD22/2000 syringe pump (Harvard Apparatus, MA) for an additional 24 h.

### Cell Survival, Proliferation, and Morphology

Before exposure to shear flow, the cells were stained with propidium iodide (PI; Sigma-Aldrich) at 37°C for 10 min. Images were acquired using confocal laser-scanning microscopy (Zeiss LSM880, Germany) from five fields of view (FOVs) randomly selected. Total and dead cells were counted by ImageJ software (National Institutes of Health, MD), and cell survival rate was calculated as  $1 - \text{dead cells}/\text{total cells}$ . Cell proliferation after 24-h culture was characterized by cell number per FOV compared with that at 1 h after cell seeding. To quantify cell morphology, cell area and perimeter were estimated from individual cell using ImageJ software, and cell circularity was then determined by,  $\text{cell perimeter}^2/(4\pi \times \text{cell area})$ .

### Scanning Electron Microscopy

Samples of collagen gels or collagen/cell mixtures were prepared using a combination of glutaraldehyde and ethanol dehydration followed by critical-point dried and gold coating, as described previously (45). Specimens were analyzed and photographed by environmental scanning electron microscopy (ESEM; Quanta 200, The Netherlands).

### Determination of Collagen Gel Elasticity via Rheometry

Storage modulus ( $G'$ ) of collagen gel was measured by a HAAKE rotational rheometer (RheoStress 6000, Germany). Collagen samples of 10 mm diameter were polymerized in glass disks that were later mounted onto the base plates in the rheometer. Afterward, a frequency sweep from 0.1 to

10 Hz was applied to the gels at 0.1% strain under ambient conditions. The storage modulus value measured at 1 Hz was reported as the storage modulus for a specific gel formulation.

### Immunofluorescence Staining

After the chip was disassembled, C3A or HepG2 cells were fixed, permeabilized, and blocked with 1% BSA. The cells were then incubated with primary Alexa Fluor 647-conjugated anti-cytokeratin 18 (CK18) monoclonal antibodies (mAbs), FITC-conjugated anti-CD31 mAbs, rabbit anti-cluster of differentiation 146 (CD146) mAbs, chicken anti-albumin polyclonal antibodies (pAbs), rabbit anti-cytochrome P450 (CYP450) reductase pAbs, or mouse anti-hepatocyte nuclear factor 4  $\alpha$  (HNF4 $\alpha$ ) mAbs (all primary antibodies were purchased from Abcam, MA) at 37°C for 1 h. For those stained with nonconjugated primary antibodies, the cells were further incubated with secondary Alexa Fluor 647-conjugated anti-rabbit pAbs (Abcam), Alexa Fluor 594-conjugated anti-chicken pAbs (Abcam), Alexa Fluor 488-conjugated anti-rabbit pAbs (Abcam), or Alexa Fluor 647-conjugated anti-mouse pAbs (Cell Signaling Technology, MA) for 1 h at 37°C. Immunofluorescence images of stained cells were examined using confocal laser-scanning microscopy (Zeiss LSM710, Germany). Average fluorescence intensity was determined by total intensity divided by total cell area per FOV after background subtraction using threshold segmentation with ImageJ software.

### ELISA

Supernatants were collected from the chip after 24 h of flow experiment and centrifuged to remove cell debris. Human and mouse albumin levels were measured using the Human and Mouse Albumin ELISA Quantitation kit (Bethyl Laboratory, TX), respectively, according to the manufacturer's instructions.

### Diffusivity Analysis

To mimic mass transport, we introduced into the upper channel (under shear stresses of 0, 0.1, or 1.0 dyn/cm<sup>2</sup>) FITC-labeled dextran particles (10 kDa, 1 mg/mL, ~3.3 nm in diameter; Sigma-Aldrich), green fluorescence (470/505)-labeled beads (30 nm in diameter; Sigma-Aldrich), or red fluorescence (538/584)-labeled beads (100 nm in diameter; Sigma-Aldrich) in phosphate-buffered saline (PBS). Perfusion duration was set to be 10 min for dextran particles, 1 h for 30-nm beads, and 2 h for 100-nm beads to maximize their dispersion. Diffusion of these fluorescent particles into the lower channel was imaged slice by slice, with a total height of 100 µm in the Z-direction, by confocal laser-scanning microscopy (Zeiss LSM880). Fluorescence intensity of each slice was summed up to characterize the diffusivity of fluorescent particles.

### Statistical Analysis

$P$  values were calculated using the two-tailed  $t$  test for any two groups if passing the normality test (Shapiro–Wilk), or using Mann–Whitney test if not. For multiple group comparisons, we implemented the one-way ANOVA test followed by the Holm–Sidak test or the two-way ANOVA test followed by Dunn's test. Statistical significance was set at  $P < 0.05$ .

## RESULTS

### Characterization of the In Vitro Fibrotic 3D Liver Sinusoidal Model

To explore the coupling effects of matrix stiffness and shear stresses on HC functions, a fibrotic 3-D liver sinusoidal model was developed with a porous membrane inserted between upper and lower channels (Fig. 1A). The upper channel lined with LSECs mimicked liver sinusoids, whereas the lower channel represented the space of Disse. The porous membrane was used to protect HCs from direct stresses and to contribute to medium exchange (47). The HCs premixed with collagen I at various concentrations were inoculated into the lower channel, representing different stages from normal liver to cirrhosis. In fact, C3A cells grew up well within collagen gels (Fig. 1B), where highly concentrated collagen I formed a denser fiber network with a smaller pore size and lower porosity. It seemed that those cellular protrusions overlapped with collagen fibrils (white arrows) and that the density of collagen fibers around cells (red boxes) was smaller than those far away from the cells (yellow boxes) (Fig. 1B, bottom) or those without cells seeding (Fig. 1B, top). These results suggested that embedded cells interacted with the surrounding collagen fibers and remodeled the collagen network slightly. The storage moduli of collagen gels at various concentrations used were determined by a rotational rheometer. As collagen concentration increased from 1 to 7.5 mg/mL, the matrix stiffness increased from 7 to 103 Pa (Fig. 1C). Moreover, both C3A cells and HSECs presented high viability (survival rate > 90% after 24 h) at all collagen concentrations (Fig. 1D). After 24-h incubation, the number of C3A cells remained nearly unchanged (Fig. 1E), whereas that of HSECs increased slightly without significant differences (Fig. 1F). At high collagen concentration, C3A cells yielded less spreading (Fig. 1G) and rounder shape (Fig. 1H) as reported (48). In addition, the cells maintained the expressions of HC-specific CK18 and LSEC-specific CD146 inside the model (Fig. 1I), together with little expression of capillarization-specific CD31 in HSECs (data not shown). These results in Fig. 1 indicated

that the model was well established for mimicking the progresses of liver fibrosis.

### Effects of Matrix Stiffness and Shear Stresses on HC Functions

In vivo, lined LSEC monolayer and ECM presence in the space of Disse separate sinusoidal flow physically from HC. During liver fibrogenesis, ECM is largely deposited around HCs and thus mass transport (including soluble nutrients and cytokines or dissolved oxygen) to HCs becomes difficult owing to high ECM resistance against interstitial flow (49). To mimic this pathological process and test the effects of matrix stiffness and shear flow, the lower channel in the device was inoculated with C3A cells premixed with collagen I solution at a concentration of 1.0, 2.5, 5.0, or 7.5 mg/mL, and the upper channel was continuously perfused with culture medium starting from *day 2* of culture under shear stresses of 0.1, 0.5, or 1.0 dyn/cm<sup>2</sup>. Data indicated that albumin production was higher than static cultures when the coculture system was subjected to shear stresses, followed by a descending phase once shear stresses were further increased (Fig. 2; Table 1). At extremely high collagen concentration (7.5 mg/mL), this flow-enhanced pattern was no longer observed (“NS” in Table 1) presumably because of the difficulties of fluid flow penetrating through a highly dense collagen network. In addition, C3A cells embedded in collagen gels of higher concentration produced less albumin in the presence or absence of shear stresses, consistent with previous reports (24). Similarly, this collagen I-enhanced pattern was relatively depressed at an extremely high shear stress (1.0 dyn/cm<sup>2</sup>), as a high flow provided large forces to enforce the fluid passing through collagen network (“NS” in Table 1).

Moreover, the respective roles of matrix stiffnesses and shear stresses in downregulating albumin production seemed complementary, that is, exposure of HC to high-level stiffness with low-level shear induced an albumin production similar to that at low-level stiffness with high-level shear (dotted boxes in Fig. 2B). At high matrix stiffnesses or shear stresses, the difference in albumin production induced by either matrix stiffnesses or shear stresses was mitigated, presenting a

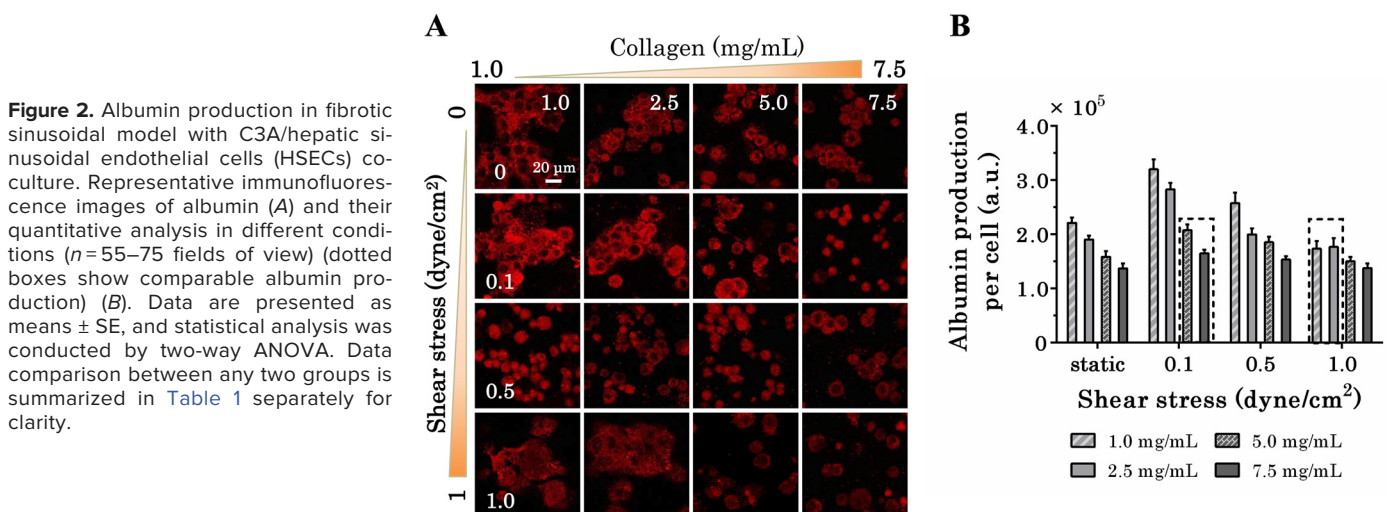


**Figure 2.** Albumin production in fibrotic sinusoidal model with C3A/hepatic sinusoidal endothelial cells (HSECs) coculture. Representative immunofluorescence images of albumin (A) and their quantitative analysis in different conditions ( $n = 55-75$  fields of view) (dotted boxes show comparable albumin production) (B). Data are presented as means  $\pm$  SE, and statistical analysis was conducted by two-way ANOVA. Data comparison between any two groups is summarized in Table 1 separately for clarity.

**Table 1.** Comparisons of albumin production among various conditions

Cases	Varied Collagen I Concentrations or Shear Stresses			
Shear stress, dyn/cm <sup>2</sup>	1.0 mg/mL	2.5 mg/mL	5.0 mg/mL	7.5 mg/mL
Static vs. 0.1	***	***	*	NS
Static vs. 0.5	*	NS	NS	NS
Static vs. 1.0	**	NS	NS	NS
0.1 vs. 0.5	***	***	NS	NS
0.1 vs. 1.0	***	***	**	NS
0.5 vs. 1.0	***	NS	NS	NS
Collagen I concentration, mg/mL	Static	0.1 dyn/cm <sup>2</sup>	0.5 dyn/cm <sup>2</sup>	1.0 dyn/cm <sup>2</sup>
1.0 vs. 2.5	NS	*	**	NS
1.0 vs. 5.0	***	***	***	NS
1.0 vs. 7.5	***	***	***	NS
2.5 vs. 5.0	NS	***	NS	NS
2.5 vs. 7.5	**	***	*	NS
5.0 vs. 7.5	NS	*	NS	NS

\**P* < 0.05, \*\**P* < 0.01, \*\*\**P* < 0.001. NS, not significant.

saturation manner of mechanical regulation (Fig. 2). These results suggested that both mechanical factors correlated with HCs' albumin production.

**Correlation of Shear Stresses with Flow-Induced Mass Transport in HC Functions**

In the above C3A/LSEC coculture system, LSECs were exposed to shear stresses directly, which might regulate HC functions via either paracrine signaling or physical barrier. Here, we just focused on elucidating the potential role of physical barrier, as hepatocyte growth factor (HGF) secretion is highly prohibited in HSEC cell lines (data not shown) even though it is expressed in primary mouse LSECs (45). At least two sources of the physical barrier existed in the current work. First, to eliminate the effect of LSEC barrier, a simplified fibrotic sinusoidal model containing C3A cells alone was constructed. Collected data indicated similar patterns of mechanical regulation compared with the coculture system. That is, stiff matrix weakened the albumin production and

shear stresses presented biphasic effects where low shear promoted but high shear inhibited albumin production (Fig. 3, A and C). This finding was consistent with an independent ELISA of albumin secretion from C3A cells that were cultured in this model alone (Supplemental Fig. S1A; all supplemental material is available at <https://doi.org/10.6084/m9.figshare.11448348>), presenting a similar pattern of biomechanically induced albumin expression. Moreover, the albumin production of mouse primary HCs further confirmed the above responses to matrix stiffness or shear stress (Supplemental Fig. S1B). These observations were supported by CYP450 reductase expression in similar downregulation of matrix stiffness and biphasic effects of shear stresses (Fig. 3, B and D). CYP450 reductase is a necessary reductant for almost all P450 reactions, and its production could serve as the readout of nearly all the CYP isoenzymes expression (50). Moreover, these regulating patterns seemed universal in various cell lines, as replacing C3A cells with HepG2 cells (51) resulted in similar effects of matrix stiffness or shear stresses on albumin production and CYP450 reductase expression

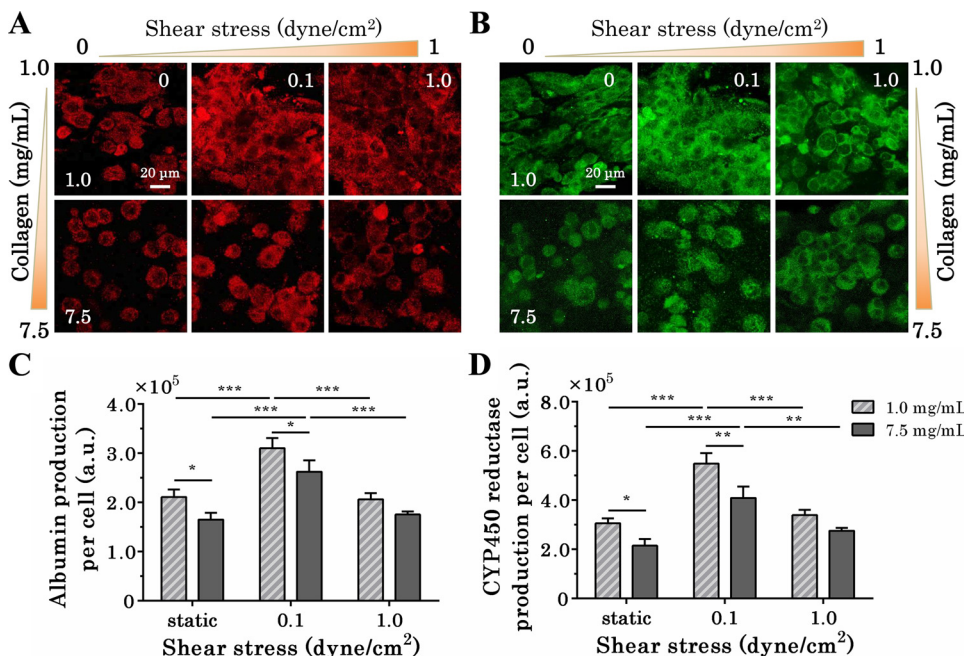


**Figure 3.** Production of albumin and cytochrome P450 (CYP450) reductase in fibrotic sinusoidal model with C3A cells alone. Immunofluorescence images of C3A cells stained by albumin (A) and CYP450 reductase (B). Production of albumin (C) or CYP450 reductase (D) was quantified from the images (*n* = 45–60 fields of view). Data are presented as means ± SE, and statistical analysis was conducted by two-way ANOVA. \**P* < 0.05, \*\**P* < 0.01, and \*\*\**P* < 0.001.



(Supplemental Fig. S2, A and B). The second source came from collagen I network that presented between two channels to provide a 3-D ECM microenvironment and abundant adhesive sites for cell growth. Data were thus collected from C3A cells cultured in a collagen I-free model, presenting a similar pattern that only appropriate level of shear stresses favored albumin production and CYP450 reductase expression (Supplemental Fig. S2, C and D).

Another key factor in modulating mass transport is the pressure gradient of fluid flow, which is governed by flow rate and model geometry. To test this, the heights of upper and lower channels were reduced from 100 to 50  $\mu\text{m}$ . Typical data from C3A cells embedded in low-concentration collagen gel indicated a distinct regulating pattern of shear stresses, that is, albumin production and CYP450 reductase expression were likely increased with an increase in shear stresses. By contrast, high matrix stiffness still downregulated albumin production and CYP450 reductase expression at low shear stresses, as expected (Supplemental Fig. S3). Thus, mechanical regulation of matrix stiffness and shear stresses in typical HC functions was mainly attributed to the driving force and physical barrier in the model proposed here.

### Particle Diffusivity in the Cell-Containing Collagen Network

Sinusoidal blood flow favors transferring nutrients, growth factors, or cytokines to HCs and brings their metabolic waste away from sinusoids in normal liver. However, the knowledge on how the flow changes in the fibrotic liver is yet unknown. We introduced FITC-labeled dextran particles, green fluorescence-labeled beads (30 nm in diameter), or red fluorescence-labeled beads (100 nm in diameter) into the upper channel to mimic the flow-enforced diffusion of biomolecules or even molecule clusters toward cell-containing lower channel under varied collagen I concentrations or shear stresses (Fig. 4A). Diffusivity analysis indicated that as the collagen concentration increased, both dextran particles and two types of beads' diffusivity dropped significantly, as expected (Fig. 4, B–D). Tests of static diffusivity of both beads yielded very low values compared with shear stresses-induced diffusivity and presented no difference between low and high collagen I concentrations (Fig. 4, C and D). Hence, shear stresses could be a key factor that promotes distinct roles of varied collagen gels in mass transport. As shear

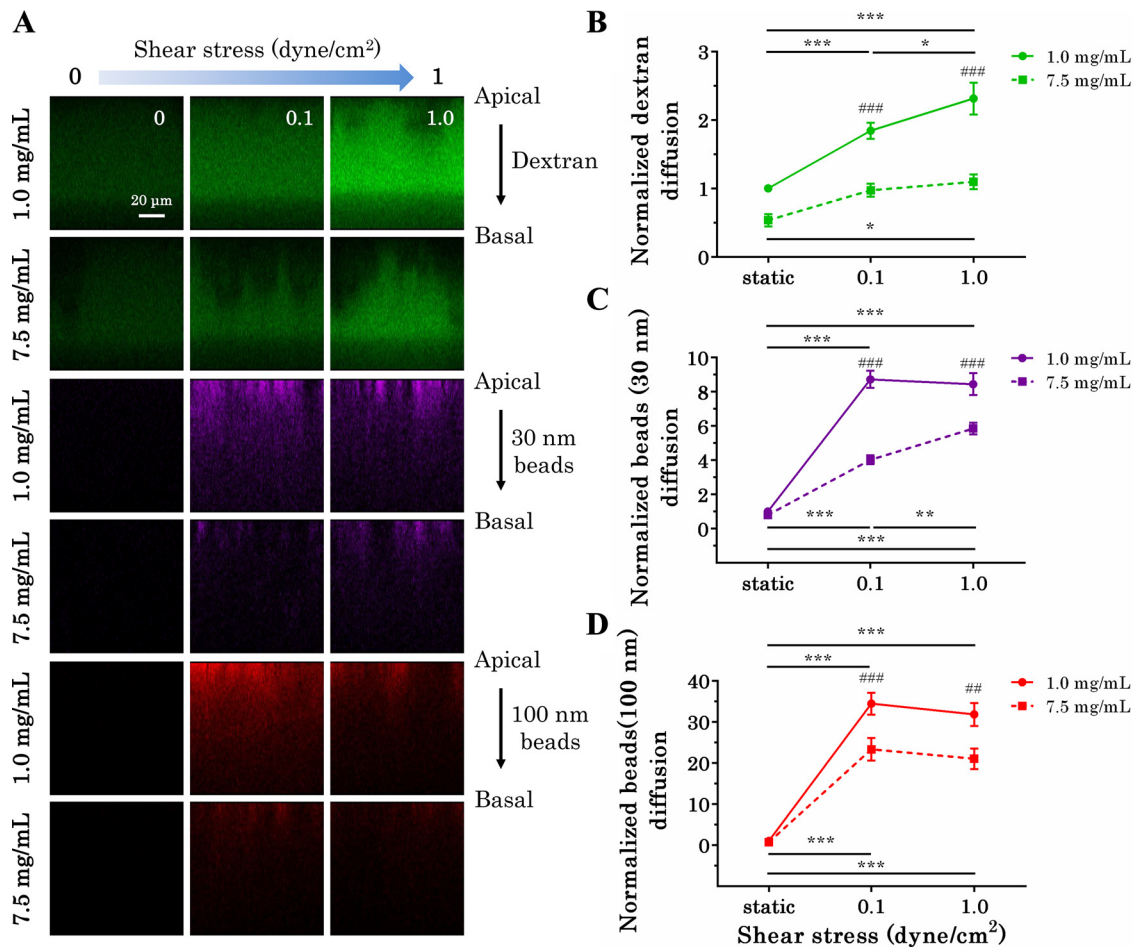


**Figure 4.** Diffusivity analysis of porous collagen network in a fibrotic sinusoidal model. A: dextran particles (green), 30-nm beads (purple), or 100-nm beads (red) were forced to diffuse across porous membrane from the upper channel toward the lower channel. Mass transports of dextran particles (B), 30-nm beads (C), or 100-nm beads (D) were monitored in various conditions ( $n = 20\text{--}35$  fields of view). Data are presented as means  $\pm$  SE of measured fluorescence intensity (a. u.) along the apical-basal axis, and statistical analysis was conducted by two-way ANOVA.  $\#\#P < 0.01$ ,  $\#\#\#P < 0.001$  compared with 7.5 mg/mL group under corresponding shear stresses.  $*P < 0.05$ ,  $**P < 0.01$ , and  $***P < 0.001$ .

stresses increased, dextran particle permeability increased persistently, whereas 100-nm beads permeability increased first, and then tended to decrease (Fig. 4, B and D). Interestingly, 30-nm beads exhibited similar permeability with dextran particles at high collagen I concentration and with 100-nm beads at low collagen I concentration (Fig. 4C). These results suggested that transporting molecules with different sizes presented various diffusion activities through porous collagen networks, and the diffusion of large-sized molecules yielded the same pattern with albumin production in response to shear stresses (cf. Fig. 3C).

### Role of HNF4 $\alpha$ Signaling in Mechanical Regulation

To explore the underlying mechanisms of mechanical regulation, a typical liver-specific and mechanosensitive signaling molecule was tested. Here, HNF4 $\alpha$  expressions were quantified in various conditions (23). The stiff matrix inhibited HNF4 $\alpha$  expression except at the high shear stress of 1.0 dyn/cm<sup>2</sup>, consistent with a reduced albumin production at high matrix stiffness (Fig. 5, A and B). Shear flow promoted HNF4 $\alpha$  expression in the current setting of shear stresses (Fig. 5B). These data suggest that HNF4 $\alpha$  might be a potential factor for modulating HC functional responses to matrix stiffness. By contrast, shear stress-induced biphasic effects on HC functions (cf. Fig. 3) might not be attributed to HNF4 $\alpha$  signaling alone, as no biphasic features were observed.

## DISCUSSION

The goal of the current work is to elucidate the mechanical regulation of liver-specific functions during liver fibrosis. A microfluidic device that mimics the anatomical architecture of a fibrotic 3-D liver sinusoidal module was developed to study the microenvironment impact of matrix stiffness and shear stresses on HC functions. This in vitro model enabled controlled tests with various mechanical parameters of matrix stiffness and/or shear stresses independently or simultaneously. Mixing HC with collagen I solution at different concentrations before gelation yielded a well-controlled matrix stiffness that mimics the deposition of collagen I-rich ECM during the liver fibrosis process. Installation of a porous PET membrane between the two channels helps to form a high flow velocity environment for efficient mass transport with low shear stresses to protect HC from direct shear force (52), favoring the balance between sufficient nutrient supply and minimized shear perturbation. Moreover, although the

pore size of PET membrane is usually >1 $\mu$ m in diameter in the literatures (42, 52–55), the much smaller-sized pores (0.4 $\mu$ m) on PET membrane used here are more suitable to represent the fenestrae and gaps in LSEC (45, 56). Thus, this well-defined microfluidic chip provides an in vitro liver sinusoid model to explore the isolated or coupled effects of the two mechanical factors, matrix stiffness and shear stresses, on HC functions.

Evidently, matrix stiffness is the first mechanical variation in liver fibrosis. Mechanical measurements of human bulk liver tissues using oscillatory rheometry revealed stiffness values in the range of 0.4–0.6 kPa for the normal liver and ~1.2–1.6 kPa for the fibrotic liver (23). These values were evidently larger than the stiffness of collagen gels used in present study, as these large values represented the tissue rigidity rather than matrix stiffness like collagen I component. Presently, the stiffest collagen gel demonstrated >10-fold increase in its storage modulus compared with the softest one, which was sufficient to mimic the mechanical changes during liver fibrosis due to ECM deposition.

Biomechanically, high matrix stiffness represents a dense collagen network, providing high resistance to flow-induced mass transport (49). Biochemically, high substrate stiffness improves cell adhesion, viability, and cytoskeletal organization but depresses liver-specific gene expressions of Baat, Gys2, and F7 through HNF4 $\alpha$  (23, 24). This result is consistent with our results that stiffer matrix with high collagen concentration downregulates the expressions of albumin, CYP450 reductase, and HNF4 $\alpha$  collectively. Stiffer substrates might also promote HC proliferation and liver fibrosis through a decrease in HNF4 $\alpha$  (57–59). Therefore, this work proposed an HNF4 $\alpha$ -involved potential positive-feedback pathway in the development of liver cirrhosis. Matrix stiffness in the liver could serve as a potential therapeutic target, as observed in the treatment of stage F3–F4 liver fibrosis with the inhibitors of collagen condensation in previous study (60).

Blood flow is another mechanical factor necessarily required for the retention of HC phenotype and functions. It has been suggested that HC can sense the shear stresses via the microvilli at their sinusoidal surface (61). They are quite sensitive to shear stresses, as they react differently at varied shear amplitudes and even the same level of shear stresses. For instance, ammonia metabolic and urea synthetic activities as well as alanine aminotransferase (ALT) release are enhanced synchronously after 24-h culture of HC that are exposed to a shear stress of 1.3 dyn/cm<sup>2</sup> in the flow chamber

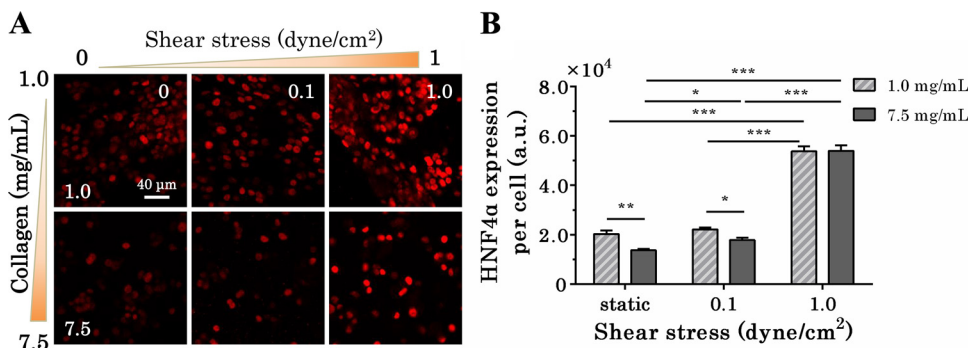


**Figure 5.** Hepatocyte nuclear factor 4 $\alpha$  (HNF4 $\alpha$ ) expression in fibrotic sinusoidal model with C3A cells alone. Typical immunofluorescence images of HNF4 $\alpha$  expression (A) and their quantitative analysis in various conditions ( $n=60$  fields of view) (B). Data are presented as means  $\pm$  SE, and statistical analysis was conducted by two-way ANOVA. \* $P < 0.05$ , \*\* $P < 0.01$ , and \*\*\* $P < 0.001$ .



(41). Dynamic medium flow (DMF)-culturing substantially increases the detoxification properties and bile acid production of HepaRG cells at a flow rate of 5 mL/min, whereas lower or higher flow rates result in decreased functionality and increased cell damage (62), which are consistent with the results performed using HepaRG-AMC-bioartificial liver (63). Occasionally, only extreme low shear stresses are favorable in the perfusion culture of mouse or pig fetal liver cells immobilized within a 3-D porous scaffold (64). Therefore, shear flow likely presents biphasic effects on HC functions. The observations that high shear flow is detrimental for HC functions may result from the suprphysiological flow, as in vivo shear stresses are  $\sim 0.1$  to  $0.5$  dyn/cm<sup>2</sup> within sinusoid vessels (65). Our results support that the effects of shear flow on HC could be biphasic, as seen in the enhanced albumin production at  $0.1$  dyn/cm<sup>2</sup> but in the reduced production at  $1.0$  dyn/cm<sup>2</sup>. Therefore, the changes in shear stresses during liver fibrogenesis or liver resection can affect liver function directly, highlighting the therapeutic potential of drugs or surgical procedures to manipulate shear stresses.

In addition to the direct effects on HC, shear flow is able to distribute those soluble factors of oxygen, nutrition, cytokines, or metabolites approaching to or flowing away from HC. In this work, diffusivity analysis of fluorescent particles suggests that mass transport contributed to this shear-induced effect. The resulted distribution is mainly determined by shear stresses, porosity of collagen network, and model geometry.

Responses of HC to mechanical cues are critical to liver-specific functions. Although shear stresses either enhance or impair HC that are directly exposed to shear flow, it is still unclear for the underlying mechanisms since in vivo blood flows across the endothelial cells with indirect contact with the HC. It is also unknown how the ECM matrix underneath the endothelium alters the fluid flow or the shear stresses, especially in cases of fibrotic or cirrhotic HCs. Our results indicate that HCs maintained similar responses to shear stresses in the presence or absence of ECM matrix (Fig. 3 and Supplemental Fig. S2, C and D), implying that shear stress-induced effects on HCs were not affected by collagen gels. Interpretation of this unexpected observation depends on the actual level of shear stresses around the cells, which is quite complicated and hard to define locally. A simple test of reducing channel height presented a distinct pattern of flow-induced albumin production (cf. Supplemental Fig. S3), also consistent with those observations that optimal shear stresses vary in different models or modules (62, 66).

Although the current work provides a flexible platform with a coculture of HCs and LSECs to understand the fibrotic progress and the related mechanical regulation, it is still an in vitro laboratory model. Future robust models will mimic the in vivo sinusoids by addition of immune cells and HSCs/myofibroblasts. In addition, only collagen I was adopted previously to elucidate the effects of matrix stiffness on HC functions during fibrotic progresses, as it is the major component of interstitial matrix surrounding cells (67, 68) and its expression level has been used for diagnosing and staging liver fibrosis (69). It should be noted that a limited subset of integrins/matrix receptors serves as mechanosensors between collagen scaffold and cytoskeleton, which might affect cellular mechanotransduction

(70). Moreover, integrating computational fluid dynamics analysis with particle imaging velocimetry test would elaborate the global and local flow field inside the model, unraveling the flow-induced sensitivity of HC functions and the actual fluid effects through collagen network.

## CONCLUSIONS

A fibrotic 3-D liver sinusoidal model that mimics the key architecture of the sinusoids has been developed. This model provides a powerful platform to implement liver-specific functions, and thereby, enabled the exploration of isolated or cooperating effects of the matrix stiffness and shear stresses on HC functions. Stiffer matrices suppressed typical HC functions, whereas shear stresses exhibited biphasic effects in this regard. Moreover, matrix stiffness and shear stresses regulated HC functions synergically. These observations were likely attributed to flow-enhanced mass transport or a key mechanosensitive signaling molecule of HNF4 $\alpha$ . This engineered model enabled us to elucidate the effects of mechanical factors on HC functions and to unravel the key roles of mass transport in fibrotic progresses in vitro.

## GRANTS

This work was supported by National Natural Science Foundation of China Grants 91642203, 31627804, 31661143044, 31870930; Strategic Priority Research Program, Frontier Science Key Project, and the Scientific Instrument Developing Project of Chinese Academy of Sciences Grants QYZDJ-SSW-JSC018, XDB22040101, and GJJSTU20190005.

## DISCLOSURES

No conflicts of interest, financial or otherwise, are declared by the authors.

## AUTHOR CONTRIBUTIONS

W.L., N.L., S.L., and M.L. conceived and designed research; W.L., P.L., and Y.D. performed experiments; W.L., P.L., and N.L. analyzed data; W.L. and N.L. interpreted results of experiments; W.L. prepared figures; W.L. drafted manuscript; W.L., N.L., D.E., and M.L. edited and revised manuscript; W.L., P.L., N.L., Y.D., S.L., D.E., and M.L. approved final version of manuscript.

## REFERENCES

1. Clay NE, Shin K, Ozcelikkale A, Lee MK, Rich MH, Kim DH, Han B, Kong H. Modulation of matrix softness and interstitial flow for 3D cell culture using a cell-microenvironment-on-a-chip system. *ACS Biomater Sci Eng* 2: 1968–1975, 2016. doi:10.1021/acsbomaterials.6b00379.
2. Yang H, Li N, Du Y, Tong C, Lu S, Hu J, Zhang Y, Long M. Neutrophil adhesion and crawling dynamics on liver sinusoidal endothelial cells under shear flow. *Exp Cell Res* 351: 91–99, 2017. doi:10.1016/j.yexcr.2017.01.002.
3. Poisson J, Lemoine S, Boulanger C, Durand F, Moreau R, Valla D, Pe R. Liver sinusoidal endothelial cells: physiology and role in liver diseases. *J Hepatol* 66: 212–227, 2017. doi:10.1016/j.jhep.2016.07.009.
4. Vollmar B, Menger MD. The hepatic microcirculation: mechanistic contributions and therapeutic targets in liver injury and repair. *Physiol Rev* 89: 1269–1339, 2009. doi:10.1152/physrev.00027.2008.
5. Tsuchida T, Friedman SL. Mechanisms of hepatic stellate cell activation. *Nat Rev Gastroenterol Hepatol* 14: 397–411, 2017. doi:10.1038/nrgastro.2017.38.

6. Wynn TA, Ramalingam TR. Mechanisms of fibrosis: therapeutic translation for fibrotic disease. *Nat Med* 18: 1028–1040, 2012. doi:10.1038/nm.2807.
7. Batailler R, Brenner DA. Liver fibrosis. *J Clin Invest* 115: 209–218, 2005. [Erratum in *J Clin Invest* 115: 1100, 2005]. doi:10.1172/JCI24282.
8. Friedman SL. Molecular regulation of hepatic fibrosis, an integrated cellular response to tissue injury. *J Biol Chem* 275: 2247–2250, 2000. doi:10.1074/jbc.275.4.2247.
9. Seki E, Schwabe RF. Hepatic inflammation and fibrosis: functional links and key pathways. *Hepatology* 61: 1066–1079, 2015. doi:10.1002/hep.27332.
10. Lee UE, Friedman SL. Mechanisms of hepatic fibrogenesis. *Best Pract Res Clin Gastroenterol* 25: 195–206, 2011. doi:10.1016/j.bpg.2011.02.005.
11. Pellicoro A, Ramachandran P, Iredale JP, Fallowfield JA. Liver fibrosis and repair: immune regulation of wound healing in a solid organ. *Nat Rev Immunol* 14: 181–194, 2014. doi:10.1038/nri3623.
12. Orbach SM, Ford AJ, Saverot SE, Rajagopalan P. Multi-cellular transitional organotypic models to investigate liver fibrosis. *Acta Biomater* 82: 79–92, 2018. doi:10.1016/j.actbio.2018.10.010.
13. Wells RG. Tissue mechanics and fibrosis. *Biochim Biophys Acta* 1832: 884–890, 2013. doi:10.1016/j.bbadis.2013.02.007.
14. Li Z, Gong Y, Sun S, Du Y, Lu D, Liu X, Long M. Differential regulation of stiffness, topography, and dimension of substrates in rat mesenchymal stem cells. *Biomaterials* 34: 7616–7625, 2013. doi:10.1016/j.biomaterials.2013.06.059.
15. Wang J, Lu D, Mao D, Long M. Mechanomics: an emerging field between biology and biomechanics. *Protein Cell* 5: 518–531, 2014. doi:10.1007/s13238-014-0057-9.
16. You Z, Zhou L, Li W, Huang C, Du Y. Mechanical microenvironment as a key cellular regulator in the liver. *Acta Mech Sin* 35: 289–298, 2019. doi:10.1007/s10409-019-00857-y.
17. Hansen LK, Wilhelm J, Fassett JT. Regulation of hepatocyte cell cycle progression and differentiation by type I collagen structure. *Curr Top Dev Biol* 72: 205–236, 2006.
18. Wells RG. The role of matrix stiffness in regulating cell behavior. *Hepatology* 47: 1394–1400, 2008. doi:10.1002/hep.22193.
19. Ferraioli G, Tinelli CD, Bello B, Zicchetti M, Filice G, Filice C. Accuracy of real-time shear wave elastography for assessing liver fibrosis in chronic hepatitis C: a pilot study. *Hepatology* 56: 2125–2133, 2012. doi:10.1002/hep.25936.
20. Venkatesh SK, Ehman RL. Magnetic resonance elastography of liver. *Magn Reson Imaging Clin N Am* 22: 433–446, 2014. doi:10.1016/j.mric.2014.05.001.
21. Georges PC, Hui JJ, Gombos Z, McCormick ME, Wang AY, Uemura M, Mick R, Janmey PA, Furth EE, Wells RG. Increased stiffness of the rat liver precedes matrix deposition: implications for fibrosis. *Am J Physiol Gastrointest Liver Physiol* 293: G1147–G1154, 2007. doi:10.1152/ajpgi.00032.2007.
22. Yeh WC, Li PC, Jeng YM, Hsu HC, Kuo PL, Li ML, Yang PM, Lee PH. Elastic modulus measurements of human liver and correlation with pathology. *Ultrasound Med Biol* 28: 467–474, 2002. doi:10.1016/S0301-5629(02)00489-1.
23. Desai SS, Tung JC, Zhou VX, Grenet JP, Malato Y, Rezvani M, Espanol-Suner R, Willenbring H, Weaver VM, Chang TT. Physiological ranges of matrix rigidity modulate primary mouse hepatocyte function in part through hepatocyte nuclear factor 4 alpha. *Hepatology* 64: 261–275, 2016. doi:10.1002/hep.28450.
24. Deegan DB, Zimmerman C, Skardal A, Atala A, Shupe TD. Stiffness of hyaluronic acid gels containing liver extracellular matrix supports human hepatocyte function and alters cell morphology. *J Mech Behav Biomed Mater* 55: 87–103, 2016. doi:10.1016/j.jmbbm.2015.10.016.
25. Baffy G. Origins of portal hypertension in nonalcoholic fatty liver disease. *Dig Dis Sci* 63: 563–576, 2018. doi:10.1007/s10620-017-4903-5.
26. Zhou WC, Zhang QB, Qiao L. Pathogenesis of liver cirrhosis. *WJG* 20: 7312–7324, 2014. doi:10.3748/wjg.v20.i23.7312.
27. Hu J, Lü S, Feng S, Long M. Flow dynamics analyses of pathophysiological liver lobules using porous media theory. *Acta Mech Sin* 33: 823–832, 2017. doi:10.1007/s10409-017-0674-7.
28. Wei W, Pu YS, Wang XK, Jiang A, Zhou R, Li Y, Zhang QJ, Wei YJ, Chen B, Li ZF. Wall shear stress in portal vein of cirrhotic patients with portal hypertension. *World J Gastroenterol* 23: 3279–3286, 2017. doi:10.3748/wjg.v23.i18.3279.
29. Xiao W, Shinohara M, Komori K, Sakai Y, Matsui H, Osada T. The importance of physiological oxygen concentrations in the sandwich cultures of rat hepatocytes on gas-permeable membranes. *Biotechnol Progress* 30: 1401–1410, 2014. doi:10.1002/btpr.1954.
30. Jemnitz K, Veres Z, Monostory K, Kobori L, Vereczkey L. Interspecies differences in acetaminophen sensitivity of human, rat, and mouse primary hepatocytes. *Toxicol In Vitro* 22: 961–967, 2008. doi:10.1016/j.tiv.2008.02.001.
31. Khetani SR, Bhatia SN. Microscale culture of human liver cells for drug development. *Nat Biotechnol* 26: 120–126, 2008. doi:10.1038/nbt1361.
32. Zhang JG, Ho T, Callendrello AL, Crespi CL, Stresser DM. A multi-endpoint evaluation of cytochrome P450 1A2, 2B6 and 3A4 induction response in human hepatocyte cultures after treatment with beta-naphthoflavone, phenobarbital and rifampicin. *Drug Metab Lett* 4: 185–194, 2010. doi:10.2174/187231210792928224.
33. Dash A, Inman W, Hoffmaster K, Sevidal S, Kelly J, Obach RS, Griffith LG, Tannenbaum SR. Liver tissue engineering in the evaluation of drug safety. *Expert Opin Drug Metab Toxicol* 5: 1159–1174, 2009. doi:10.1517/17425250903160664.
34. Domansky K, Inman W, Serdy J, Dash A, Lim MH, Griffith LG. Perfused multiwell plate for 3D liver tissue engineering. *Lab Chip* 10: 51–58, 2010. doi:10.1039/B913221J.
35. Powers MJ, Domansky K, Kaazempur-Mofrad MR, Kalezi A, Capitano A, Upadhyaya A, Kurzawski P, Wack KE, Stolz DB, Kamm R, Griffith LG. A microfabricated array bioreactor for perfused 3D liver culture. *Biotechnol Bioeng* 78: 257–269, 2002. doi:10.1002/bit.10143.
36. Powers MJ, Janigian DM, Wack KE, Baker CS, Beer Stolz D, Griffith LG. Functional behavior of primary rat liver cells in a three-dimensional perfused microarray bioreactor. *Tissue Eng* 8: 499–513, 2002. doi:10.1089/107632702760184745.
37. Dash A, Simmers MB, Deering TG, Berry DJ, Feaver RE, Hastings NE, Pruett TL, LeCluyse EL, Blackman BR, Wamhoff BR. Hemodynamic flow improves rat hepatocyte morphology, function, and metabolic activity in vitro. *Am J Physiol Cell Physiol* 304: C1053–C1063, 2013. doi:10.1152/ajpcell.00331.2012.
38. Xia L, Arooz T, Zhang S, Tuo X, Xiao G, Susanto TA, Sundararajan J, Cheng T, Kang Y, Poh HJ, Leo HL, Yu H. Hepatocyte function within a stacked double sandwich culture plate cylindrical bioreactor for bioartificial liver system. *Biomaterials* 33: 7925–7932, 2012. doi:10.1016/j.biomaterials.2012.06.078.
39. Esch MB, Prot JM, Wang YI, Miller P, Llamas-Vidales JR, Naughton BA, Applegate DR, Shuler ML. Multi-cellular 3D human primary liver cell culture elevates metabolic activity under fluidic flow. *Lab Chip* 15: 2269–2277, 2015. doi:10.1039/C5LC00237K.
40. Hastings NE, Simmers MB, McDonald OG, Wamhoff BR, Blackman BR. Atherosclerosis-prone hemodynamics differentially regulates endothelial and smooth muscle cell phenotypes and promotes pro-inflammatory priming. *Am J Physiol Cell Physiol* 293: C1824–C1833, 2007. doi:10.1152/ajpcell.00385.2007.
41. Kan P, Miyoshi H, Ohshima N. Perfusion of medium with supplemented growth factors changes metabolic activities and cell morphology of hepatocyte-nonparenchymal cell coculture. *Tissue Eng* 10: 1297–1307, 2004. doi:10.1089/1076327042500346.
42. Rennert K, Steinborn S, Groger M, Ungerbock B, Jank AM, Ehgartner J, Nietzsche S, Dinger J, Kiehnopf M, Funke H, Peters FT, Lupp A, Gartner C, Mayr T, Bauer M, Huber O, Mosig AS. A microfluidically perfused three dimensional human liver model. *Biomaterials* 71: 119–131, 2015. doi:10.1016/j.biomaterials.2015.08.043.
43. Larkin AL, Rodrigues RR, Murali TM, Rajagopalan P. Designing a multicellular organotypic 3D liver model with a detachable, nano-scale polymeric space of Disse. *Tissue Eng, Part C Methods* 19: 875–884, 2013. doi:10.1089/ten.tec.2012.0700.
44. Verneti LA, Senutovitch N, Boltz R, DeBiasio R, Shun TY, Gough A, Taylor DA. Human liver microphysiology platform for investigating physiology, drug safety, and disease models. *Exp Biol Med (Maywood)* 241: 101–114, 2016. doi:10.1177/1535370215592121.
45. Du Y, Li N, Yang H, Luo C, Gong Y, Tong C, Gao Y, Lu S, Long M. Mimicking liver sinusoidal structures and functions using a 3D-configured microfluidic chip. *Lab Chip* 17: 782–794, 2017. doi:10.1039/C6LC01374K.

46. **Tong CF, Zhang Y, Lü SQ, Li N, Gong YX, Yang H, Feng SL, Du Y, Huang DD, Long M.** Binding of intercellular adhesion molecule 1 to  $\beta(2)$ -integrin regulates distinct cell adhesion processes on hepatic and cerebral endothelium. *Am J Physiol Cell Physiol* 315: C409–C421, 2018. doi:10.1152/ajpcell.00083.2017.
47. **Ford AJ, Jain G, Rajagopalan P.** Designing a fibrotic microenvironment to investigate changes in human liver sinusoidal endothelial cell function. *Acta Biomater* 24: 220–227, 2015. doi:10.1016/j.actbio.2015.06.028.
48. **Zhang J, Yang H, Abali BE, Li M, Xia Y, Haag R.** Dynamic mechanics-modulated hydrogels to regulate the differentiation of stem-cell spheroids in soft microniches and modeling of the nonlinear behavior. *Small* 15: e1901920, 2019. doi:10.1002/sml.201901920.
49. **Diop-Frimpong B, Chauhan VP, Krane S, Boucher Y, Jain RK.** Losartan inhibits collagen I synthesis and improves the distribution and efficacy of nanotherapeutics in tumors. *Proc Natl Acad Sci USA* 108: 2909–2914, 2011. doi:10.1073/pnas.1018892108.
50. **Guengerich FP, Martin MV, Sohi CD, Cheng Q.** Measurement of cytochrome P450 and NADPH-cytochrome P450 reductase. *Nat Protoc* 4: 1245–1251, 2009. doi:10.1038/nprot.2009.121.
51. **Lu D, Gao Y, Luo C, Lu S, Wang Q, Xu X, Sun S, Wang C, Long M.** Selectivity of biopolymer membranes using HepG2 cells. *Regener Biomater* 2: 21–29, 2015. doi:10.1093/rb/rbu018.
52. **Ma LD, Wang YT, Wang JR, Wu JL, Meng XS, Hu P, Mu X, Liang QL, Luo GA.** Design and fabrication of a liver-on-a-chip platform for convenient, highly efficient, and safe in situ perfusion culture of 3D hepatic spheroids. *Lab Chip* 18: 2547–2562, 2018. doi:10.1039/C8LC00333E.
53. **Hegde M, Jindal R, Bhushan A, Bale SS, McCarty WJ, Golberg I, Usta OB, Yarmush ML.** Dynamic interplay of flow and collagen stabilizes primary hepatocytes culture in a microfluidic platform. *Lab Chip* 14: 2033–2039, 2014. doi:10.1039/C4LC00071D.
54. **Kostadinova R, Boess F, Applegate D, Suter L, Weiser T, Singer T, Naughton B, Roth A.** A long-term three dimensional liver co-culture system for improved prediction of clinically relevant drug-induced hepatotoxicity. *Toxicol Appl Pharmacol* 268: 1–16, 2013. doi:10.1016/j.taap.2013.01.012.
55. **Prodanov L, Jindal R, Bale SS, Hegde M, McCarty WJ, Golberg I, Bhushan A, Yarmush ML, Usta OB.** Long-term maintenance of a microfluidic 3D human liver sinusoid. *Biotechnol Bioeng* 113: 241–246, 2016. doi:10.1002/bit.25700.
56. **Li N, Zhang X, Li P, Yang H, Tong C, Lu S, Zhang Y, Ye Z, Pan J, Long M.** Mechanical strength and structural basis of  $\beta(2)$  integrin to mediate neutrophil accumulation on liver sinusoidal endothelial cells: a study using atomic force microscopy and molecular dynamics simulations. *Comput Model Eng Sci* 116: 263–279, 2018. doi:10.31614/cmescs.2018.04079.
57. **Cast A, Kumbaji M, D'Souza A, Rodriguez K, Gupta A, Karns R, Timchenko L, Timchenko N.** Liver proliferation is an essential driver of fibrosis in mouse models of nonalcoholic fatty liver disease. *Hepatal Commun* 3: 1036–1049, 2019. doi:10.1002/hep4.1381.
58. **Schrader J, Gordon-Walker TT, Aucott RL, van Deemter M, Quaas A, Walsh S, Benten D, Forbes SJ, Wells RG, Iredale JP.** Matrix stiffness modulates proliferation, chemotherapeutic response, and dormancy in hepatocellular carcinoma cells. *Hepatology* 53: 1192–1205, 2011. doi:10.1002/hep.24108.
59. **Zhao J, Adams A, Weinman SA, Tikhonovich I.** Hepatocyte PRMT1 protects from alcohol induced liver injury by modulating oxidative stress responses. *Sci Rep* 9: 9111, 2019. doi:10.1038/s41598-019-45585-2.
60. **Liu L, You Z, Yu H, Zhou L, Zhao H, Yan X, Li D, Wang B, Zhu L, Xu Y, Xia T, Shi Y, Huang C, Hou W, Du Y.** Mechanotransduction-modulated fibrotic microniches reveal the contribution of angiogenesis in liver fibrosis. *Nat Mater* 16: 1252–1261, 2017. doi:10.1038/nmat5024.
61. **Song Z, Gupta K, Ng IC, Xing J, Yang YA, Yu H.** Mechanosensing in liver regeneration. *Semin Cell Dev Biol* 71: 153–167, 2017. doi:10.1016/j.semcdb.2017.07.041.
62. **Adam AAA, van der Mark VA, Donkers JM, Wildenberg ME, Oude Elferink RPJ, Chamuleau R, Hoekstra RA.** practice-changing culture method relying on shaking substantially increases mitochondrial energy metabolism and functionality of human liver cell lines. *PLoS One* 13: e0193664, 2018. doi:10.1371/journal.pone.0193664.
63. **Nibourg GA, Boer JD, van der Hoeven TV, Ackermans MT, van Gulik TM, Chamuleau RA, Hoekstra R.** Perfusion flow rate substantially contributes to the performance of the HepaRG-AMC-bioartificial liver. *Biotechnol Bioeng* 109: 3182–3188, 2012. doi:10.1002/bit.24586.
64. **Miyoshi H, Ehashi T, Kawai H, Ohshima N, Suzuki S.** Three-dimensional perfusion cultures of mouse and pig fetal liver cells in a packed-bed reactor: effect of medium flow rate on cell numbers and hepatic functions. *J Biotechnol* 148: 226–232, 2010. doi:10.1016/j.jbiotec.2010.06.002.
65. **Lalor PF, Adams DH.** Adhesion of lymphocytes to hepatic endothelium. *Mol Pathol* 52: 214–219, 1999. doi:10.1136/mp.52.4.214.
66. **Tanaka Y, Yamato M, Okano T, Kitamori T, Sato K.** Evaluation of effects of shear stress on hepatocytes by a microchip-based system. *Meas Sci Technol* 17: 3167–3170, 2006. doi:10.1088/0957-0233/17/12/S08.
67. **Karsdal MA, Daniels SJ, Holm Nielsen S, Bager C, Rasmussen DGK, Loomba R, Surabattula R, Villesen IF, Luo Y, Shevell D, Gudmann NS, Nielsen MJ, George J, Christian R, Leeming DJ, Schuppan D.** Collagen biology and non-invasive biomarkers of liver fibrosis. *Liver Int* 40: 736–750, 2020. doi:10.1111/liv.14390.
68. **Karsdal MA, Detlefsen S, Daniels SJ, Nielsen MJ, Krag A, Schuppan D.** Is the total amount as important as localization and type of collagen in liver fibrosis attributable to steatohepatitis? *Hepatology* 71: 346–351, 2020. doi:10.1002/hep.30969.
69. **Fuchs BC, Wang H, Yang Y, Wei L, Polasek M, Schühle DT, Lauwers GY, Parkar A, Sinskey AJ, Tanabe KK, Caravan P.** Molecular MRI of collagen to diagnose and stage liver fibrosis. *J Hepatol* 59: 992–998, 2013. doi:10.1016/j.jhep.2013.06.026.
70. **Zeltz C, Gullberg D.** The integrin-collagen connection—a glue for tissue repair? *J Cell Sci* 129: 653–664, 2016. [Erratum in *J Cell Sci* 129: 1284, 2016]. doi:10.1242/jcs.180992.